

## The Inhibitive Effect of Cerium Carbonate on the Corrosion of Brass in 3% NaCl Solution.

L. Babouri<sup>1</sup>, K. Belmokre<sup>1</sup>, A. Abdelouas<sup>2</sup>, J.-F. Bardeau<sup>3</sup>, Y. El Mendili<sup>2,\*</sup>

<sup>1</sup> Faculté des sciences, Département des sciences de la matière, Université du 20 aout 1955-Skikda, Algérie.

<sup>2</sup> Laboratoire SUBATECH, CNRS-IN2P3, Ecole des Mines de Nantes-Université de Nantes, 4 rue Alfred Kastler, BP 20722, 44307 Nantes cedex 03, France.

<sup>3</sup> LUNAM Université, Institut des Molécules et Matériaux du Mans, UMR CNRS 6283, Université du Maine, Avenue Olivier Messiaen, 72085 Le Mans Cedex 9, France.

\*E-mail: [elmendil@subatech.in2p3.fr](mailto:elmendil@subatech.in2p3.fr)

Received: 30 March 2015 / Accepted: 26 June 2015 / Published: 28 July 2015

We investigated the protective efficiency of a new class of ‘green’ corrosion inhibitors on Copper-Zinc alloy (Brass). The inhibition effect of cerium carbonate (CAC) on Brass in 3% NaCl solution was investigated at room temperature both by potentiodynamic polarisation and impedance spectroscopy (EIS) methods and weight loss measurements. The surface analysis was made by scanning electron microscope and micro-Raman spectroscopy. The electrochemical measurements showed that the CAC decreases the density of the corrosion current and thus acts as a mixed type inhibitor. The CAC inhibits the corrosion of Brass by blocking the active sites of the metal surface with a maximum inhibitory efficiency of 84%, obtained with the concentration of 100 ppm of the inhibitor. The corrosion rate decreased by a factor of 3.5 in the presence of CAC, suggesting that the investigated method is promising. The mechanism of inhibition effect is attributed to adsorption of Ce-hydroxides in the excess of OH<sup>-</sup> production from the cathodic reactions of water reduction and O<sub>2</sub>. This hydroxide precipitates subsequently as a barrier against the corrosion of the active regions.

**Keywords:** Brass, Cerium Carbonate, Inhibitor, Electrochemical Measurements, Raman spectroscopy.

### 1. INTRODUCTION

Copper is one of the most noble metals in common use and has excellent resistance to corrosion in the atmosphere and in fresh water. It is used in electrical and electronic applications, building constructions, machinery,... [1,2]. The corrosion properties of copper and its alloys have

attracted much attention over the years because of their important applications in various technological fields [1-3].

The addition of zinc to copper results in an increase in strength, ductility, corrosion resistance, erosion and cavitation in all natural waters including seawater. The alloys also show high resistance to chloride-induced stress corrosion cracking. Among these alloys, there may be mentioned, Brass, which is used in pipes and hoses for the transport of feed water, condensers systems and heat exchangers in various cooling water systems especially in sea water desalination plants [4-6].

The use of Brass is motivated by its excellent features such as good thermal and electrical conductivity, the deformability of plasticity, the machining and the high corrosion resistance [7]. However, Brass exposed to different environments such as ammonia and some nitrogen compounds may be subjected to zinc dissolution,[8,9] corrosion cracking [10,11] and stress corrosion [12]. When Brass undergoes corrosion, a zinc oxide layer is initially formed which passivates the Brass surface. When the Brass is exposed to aggressive anions, such as chloride ions, an insoluble film of cuprous chloride is adsorbed on the Brass surface [13,14]. The copper ions can pass into the solution by disproportionation reaction. Thus, the Brass becomes highly susceptible to pitting corrosion due to dezincification which leads to a porous layer rich in copper [15]. Several methods have been used to protect Brass surface against corrosion and particularly chemical inhibitors. The corrosion inhibitors chemicals are either organic or inorganic chemicals.

Most of organic inhibitors are heterocyclic organic compounds containing nitrogen, sulfur and/or oxygen, [16,17] for example, the aminopyrazoles, [18] the amino-thiazole, triazoles thiols [19] and benzimidazole and its derivatives [20].

The inhibition action of organic inhibitors against the brass corrosion in NaCl medium has been intensively studied and the results show high efficiency. However, the use of some organic inhibitors has been proved to be limited for several reasons: their synthesis is often very expensive and sometimes they are highly toxic and dangerous to humans and environment such as Benzotriazole.

Due to these problems, organic inhibitors are being replaced by less toxic inorganic ones. The usually inorganic inhibitors investigated for copper alloys are chromate  $\text{CrO}_4^{2-}$ , molybdate  $\text{MoO}_4^{2-}$ , tetraborate  $\text{B}_4\text{O}_7^{2-}$  and Tungstate  $\text{WO}_4^{2-}$  [21,22]. Chromate is considered as efficient corrosion inhibitor due to a formation of an oxide film on the metal surface which passivate the electrode surface, but it is also known that it can promote corrosion acting as a cathodic reactive. However, the main drawback is the toxicity of chromate anion. The logical alternative to hexavalent chromium is the molybdate and tetraborate species. Nevertheless, molybdate and tetraborate showed very low inhibition effect. Also, it is not feasible to use tungstate alone as a corrosion inhibitor due to its low oxidizing ability and high cost. Inhibitor efficiencies for these species are: 1.56% for molybdate, 51% for tetraborate and 78.6% for chromate [21]. Sodium tungstate  $\text{Na}_2\text{WO}_4$  showed the best inhibition effect on Brass corrosion at the concentration of 20 ppm and the inhibition efficiency was 77.35% [22].

The corrosion inhibition of copper and its alloys used in installations such as power generation and sea water desalination becomes an important challenge. The inhibitory action of organic and inorganic compounds, which are generally used are well known and widely described in the literature. It was found that most of them present the disadvantage of high degree of toxicity and are dangerous to humans and the environment [23].

It is now required to design new environment-friendly inhibitors. Recent researches have been oriented towards the use of corrosion inhibitors called "green" very effective, low-cost, non-toxic and biodegradable [24,25].

In this regard, studies have been made on the use of rare earths as corrosion inhibitors for various types of metals and alloys, such as aluminum, [26,27] zinc, [28,29] bronze, [30] steel [31] and manganese, [32,33] but rarely for Brass. Due to their abundance and relative low toxicity, rare earth ions are potentially interesting from an economic viewpoint [26-33].

The results reported in the literature on the use of rare earths including cerium salts showed good inhibitory efficiency which leads to the formation of a protective film consisting of oxide and hydroxide on the metal surface [34].

As a contribution to the prevention of the installations employed in a saline environment, our work report on the effectiveness of corrosion inhibition of Brass by the cerium carbonate using electrochemical measurements and surface analysis. The structural characterization was performed using the SEM/EDX and micro-Raman spectroscopies.

## 2. EXPERIMENTAL SECTION

### 2.1 Brass preparation

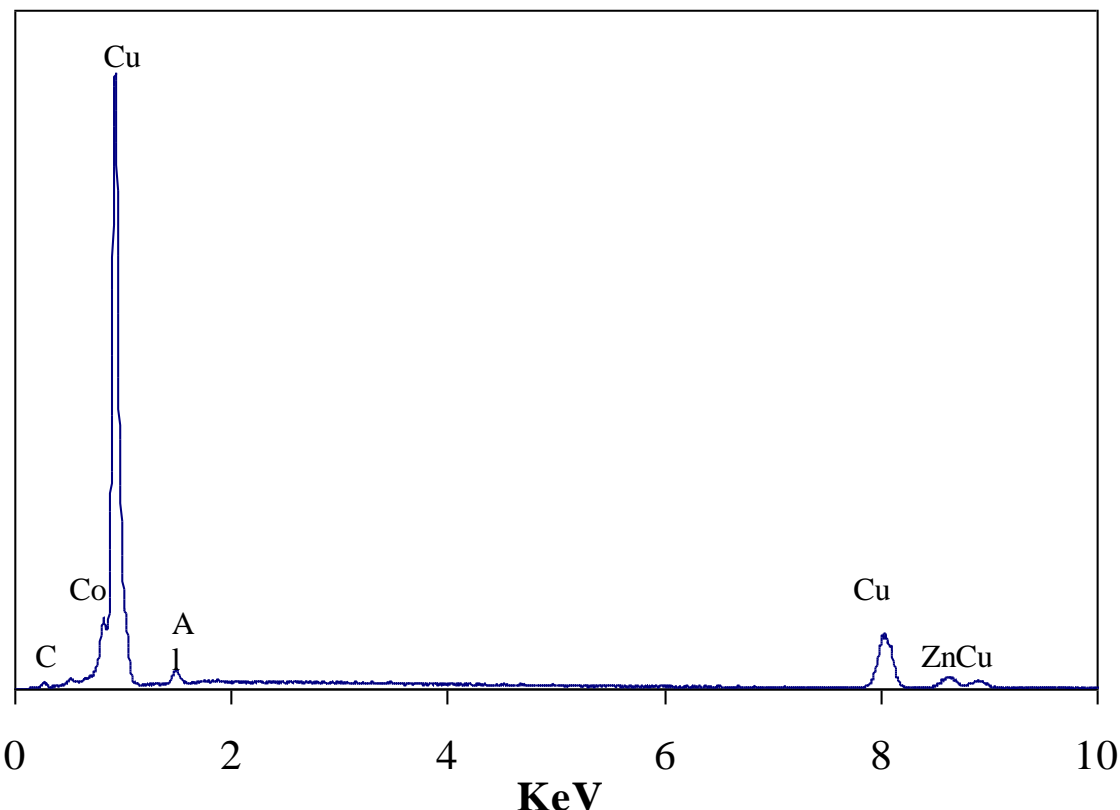


**Figure 1.** EDX spectrum of the copper-zinc alloy.

The material used in this study is a copper-zinc alloy (Brass), provided by the Skikda power plant (Algeria) and made by *SNC-Lavalin* Group Inc (Canada). This alloy is employed for sea water condenser systems and in desalination plants, as well as for piping in chemical plants.

The Brass coupons were cut into  $25 \times 25 \times 1$  mm and then polished on a  $0.3 \mu\text{m}$  PSA disc (Pressure Sensitive Adhesive disc). The coupons were cleaned according to the ASTM standard method: pickled in an uninhibited 15% HCl acid solution for 10 minutes, neutralized in a 5% solution of sodium bicarbonate and finally dried by a forced air flow before experiments.

The chemical composition of Cu-Zn alloy, as determined by EDX (Fig. 1), is 76.3% Cu, 2.9% Al, 20.7% Zn and <1 % Co.

## 2.2 Samples Preparation

The experiments were conducted at room temperature, under aerobic conditions in a 3% NaCl salt solution corresponding to NaCl concentration in seawater. The inhibitor tested is cerium carbonate  $\text{Ce}_2(\text{CO}_3)_3$ , in the form of hydrated powder. The cerium carbonate stock solution, with Ce-concentration ranging from 10 to 150 ppm, were prepared by dissolving cerium carbonate in deionized water.

## 2.3 Electrochemical analysis

The electrochemical studies were carried out using potentiostat/galvanostat (model PGZ 301). Acquisition and basic treatment of spectra have been made with the VoltaMaster 4 software connected to a thermostated double-walled electrochemical cell.

The electrochemical cell of 400 mL with cylindrical shape was used. A conventional three-electrode electrochemical cell of 400 mL was used. The cell assembly consisted of a platinum foil as counter electrode ( $C_E$ ), Ag/AgCl as reference electrode ( $R_E$ ) and of Brass as working electrode with an exposed surface area of  $1 \text{ cm}^2$  embedded in a chemically inert resin.

Before each test, the electrodes were abraded mechanically with silicon carbide papers from 400 to 4000 grit followed by polishing with diamond paste to a  $0.3\mu$  finish. The electrode was thoroughly washed with distilled water, degreased in acetone, rinsed with distilled water and dried under forced-air. The whole procedure was followed before each electrochemical experiment.

Polarization curves were obtained in a scanning field (-1000 to 800 mV) with scan rate 1 mV/s. Before polarization experiments, the open circuit potential of the working electrode was measured as a function of immersion time during 1 hour, the time necessary to reach a quasi-stationary value for the open circuit potential [35]. All curves were corrected for ohmic drop previously determined by electrochemical impedance spectroscopy.

Electrochemical impedance diagrams were made in medium 3% NaCl aerated at room temperature in the presence and absence of inhibitor, after an immersion time of one hour at open circuit. The frequency range is between 100 kHz and 10mHz using a sinusoidal signal of The electrochemical impedance diagrams were made in 3% NaCl aerated medium at room temperature

with the presence and the absence of inhibitor after immersion for one hour in an open circuit. The EIS were acquired in the frequency range from 100 kHz to 10 mHz with 10 mV amplitude sine wave generated by a frequency response analyzer. The measured parameters (perturbation amplitude and standard resistance) have been previously optimized.

## 2.4 Mass loss

### 2.4.1 Samples Preparation

The Brass coupons were cut into 1.5 \* 1.5 \* 0.08 cm, polished down to 0.3 μm and immersed in 100 ml of 3% NaCl solution containing different concentration of cerium. The aging time is 15 days at room temperature.

### 2.4.2 Surface Analysis

Scanning Electron Microscopy (SEM) coupled to Energy Dispersive Spectroscopy (EDX) was used to study the morphology and the chemical composition of brass surface. The accelerating voltage was 15 kV.

The thick layers of corrosion products have been studied by Raman spectroscopy. Raman spectra were carried out on the surface of Brass coupons which were cultured for 15 days in 3% NaCl solution at free potential and under aerated conditions. The Raman experiments were performed at room temperature using a T64000 Jobin-Yvon/Horiba spectrometer equipped with a 600 lines/mm diffraction grating and a liquid nitrogen cooled CCD detector. The Raman spectra were recorded under a microscope (Olympus Bx41) in the backscattering geometry with a 100x objective (with a spot size of about 0.8 μm) focusing the 514 nm line from an Argon–Krypton ion laser (coherent, Innova). Single spectra were systematically recorded twice in the wavenumber 100-2000 cm<sup>-1</sup> region with a very low laser power (to avoid deterioration of samples) and an integration time of 600 s. Acquisition and basic treatment of spectra have been made with the LabSpec V5.25 (Jobin Yvon-Horiba) software.

### 2.4.3 Solution Analysis

At the end of reaction time (15 days), a total volume of 1.5 mL of the solution was collected, filtered with a 0.2 μm filters for pH measurement and an chemical analyses. The technique used for quantification of Cu and Zn concentrations is Inductively Coupled Plasma-Mass Spectrometry (ICP-MS).

In static tests, calculation of normalized mass losses (NL) has been taken from the release of Cu and Zn in the following formula [36]:

$$NL_i = \frac{C_i}{X_i \left( \frac{S}{V} \right)} * 100 \quad (1)$$

With:

$C_i$  is the concentration of the element i in the solution ( $\text{g.m}^{-3}$ )

$X_i$  is the weight fraction of component i in the alloy.

(S/V) is the ratio of the area of the alloy on the volume of the solution ( $\text{m}^{-1}$ ).

#### 2.4.4 Corrosion Rate

For all experiments, the corrosion rate ( $V_{\text{corr}}$ ) was determined from the weight loss measurements according to the ASTM standard method, using the following formula:

$$V_{\text{corr}} (\mu\text{m/year}) = \frac{3650 \times \text{weight loss (mg)}}{\text{Density (g/cm}^3) \times \text{Area (cm}^2) \times \text{Time (days)}} \quad (2)$$

With a density of 8.40 g/cm<sup>3</sup> for brass

### 3. RESULTS AND DISCUSSION

#### 3.1. Electrochemical study

Before testing the protective efficiency of the cerium carbonate (CAC) inhibitor, we studied the electrochemical behavior of the Cu-Zn alloy in 3% NaCl solution. Fig. 2 shows the potentiokinetic polarization curves of Brass in 3% NaCl solution.

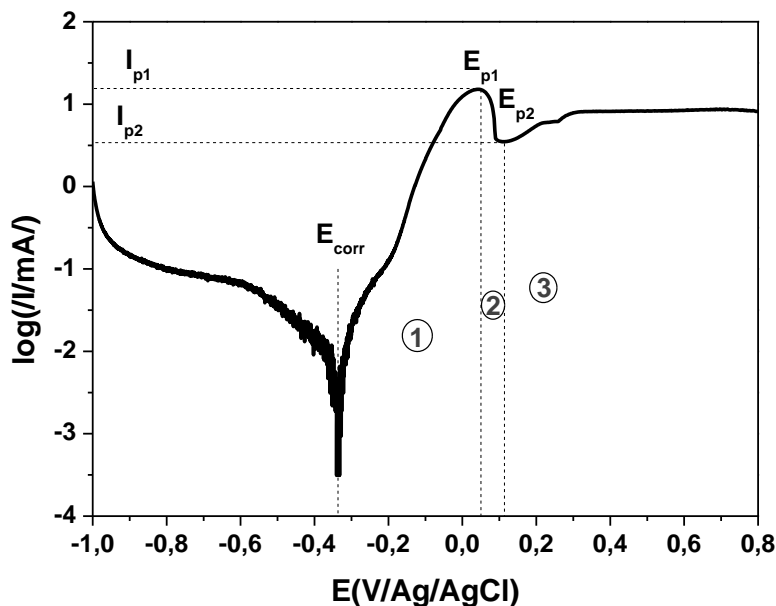
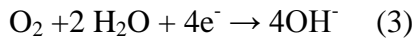


**Figure 2.** Polarization curve of Brass in 3% NaCl solution.

The analysis of the polarization curve shows that the cathodic branch is characterized by a low variation of the current density in the potential region ( $E_{\text{corr}}$  at -0.6 V) attributed to the reduction of water in the neutral 3% NaCl solution [37]:



On the anodic branch of the polarization curve, we distinguish the appearance of three zones. These zones can be described as follow:

Zone 1: characterized by a decrease of a current density followed by a strong increase in with the applied potential from ( $E_{\text{corr}} = -0.333\text{V}$ ) until reaching the maximum ( $E_{\text{p1}}$ ), which represent the active phase of Brass dissolution and thus corresponds to a critical polarization potential ( $E_{\text{p1}}=0.039\text{V}$ ).

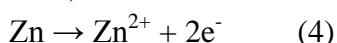
We suggest that during this phase, the transfer of cations from the metal surface to the electrolyte is the predominant phenomenon of the overall reaction as described by the Butler-Volmer equation.

Zone 2: is characterized by a drastic decrease in the dissolution current until reaching the corrosion current density in the passive state,  $I_{\text{p2}}$ . This portion of the polarization curve is the active-passive transition region (prepassivity) where the Cu-Zn alloy is covered by the corrosion products, resulting in the formation of a porous layer with low adherence properties.

Zone 3: represents the current limiting area of the curve. This zone is characterized by a small rise again from the current density from the potential ( $E_{\text{p2}} = 0.12\text{V}$ ) until the anodic limit, which corresponds to the formation of a passive layer. The rise of the current density can be explained by the rupture of the corrosion product layer exposing the Brass surface directly to electrolyte causing the migration of metallic ions to the solution.

In the anodic area, generally the reaction mechanism of the Cu-Zn alloy in the hydrogen chloride solution generates the following steps [38]:

First, the dissolution of zinc and zinc oxide formation (ZnO):



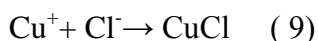
Or



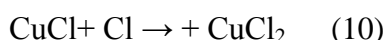
Then the dissolution of copper for the copper oxide formation  $\text{Cu}_2\text{O}$  and  $\text{CuO}$ :



When the surface is covered with ZnO, CuO and  $\text{Cu}_2\text{O}$ ,  $\text{CuCl}$  can be formed on the surface according to the reaction:



$\text{CuCl}$  undergoes self-disproportionation, or dismutation reaction [39]:



Which dissolves with the formation of the complex  $\text{CuCl}_2^-$  via the reaction (9) [40,41]:



In chloride media, other reactions involving chloride ions, namely, the formation of chloro-complex compounds may occur.

The cathodic and anodic polarization curves of Brass in 3% NaCl solution as a function of the CAC inhibitor concentrations are shown in Fig. 3. The corresponding electrochemical parameters are summarized in Table 1. The efficiency of the inhibition ( $E_i$ ) was calculated using the following equation [42]:

$$E_i(\%) = \frac{I_{\text{corr}} - I_{\text{corr(inh)}}}{I_{\text{corr}}} * 100 \quad (12)$$

Where:  $I_{\text{corr}}$  and  $I_{\text{corr(inh)}}$  represent the current densities in the absence and presence of the inhibitor, respectively.

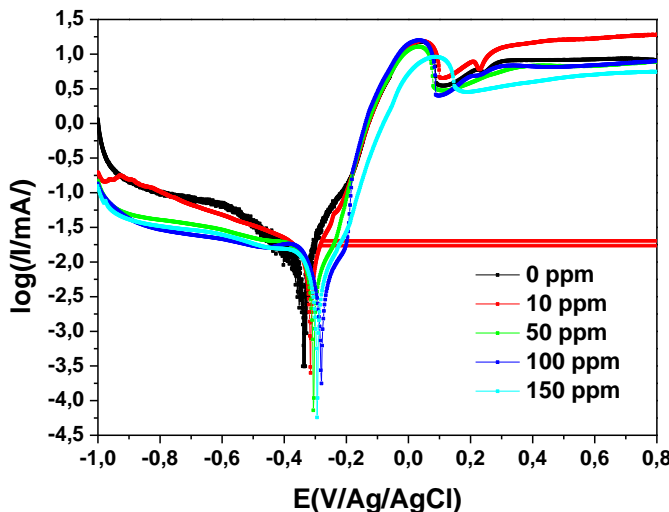


**Figure 3.** Polarization curves (E-logi) of the Brass in 3% NaCl solution in the absence and presence of different concentration of CAC inhibitor.

**Table 1.** Electrochemical parameters and the efficiency of the corrosion inhibition of Brass in 3% NaCl containing different concentrations of CAC.

Concentration of ACC inhibitor (ppm)	$I_{\text{corr}}$ ( $\mu\text{A cm}^{-2}$ )	$E_{\text{corr}}$ (mV/(Ag/AgCl))	$E_{ba}$ (mV/dec $^{-1}$ )	$E_{bc}$ (mV/dec $^{-1}$ )	$E_i$ (%)	$\Theta$
0	9.6	-333.2	109.4	311.7	-	-
10	7.4	-315.4	93.5	293.8	23%	0.23
50	3.5	-305.4	71.7	205.3	64%	0.64
<b>100</b>	<b>1.5</b>	<b>-278.2</b>	<b>55.6</b>	<b>158.8</b>	<b>84%</b>	<b>0.84</b>
150	3.8	-293.6	87.5	242.9	60%	0.60

The potentiodynamic tests, revealed that the CAC displaces the corrosion potential ( $E_{\text{corr}}$ ) to higher values. Thus, the corrosion current densities decreased increasingly also with the variation of the inhibitor concentration (up to 100 ppm), which leads to the formation of a protective film on the surface of the metal composed of oxide and cerium hydroxide [43].

The values of the cathode slope ( $b_c$ ) and the anode slope ( $b_a$ ) of Tafel curve have undergone changes with the increase of the CAC concentration. This phenomenon clearly indicates that the tested

inhibitor interferes with the anodic and cathodic reactions and significantly decreases the density of corrosion current and thus acts as a mixed type inhibitor.

Fig. 4 shows the efficiency of Brass corrosion inhibition as function of CAC inhibitor concentrations. The inhibition efficiency ( $E_i$ ) reaches a maximum value of 84% to a critical concentration of 100 ppm.

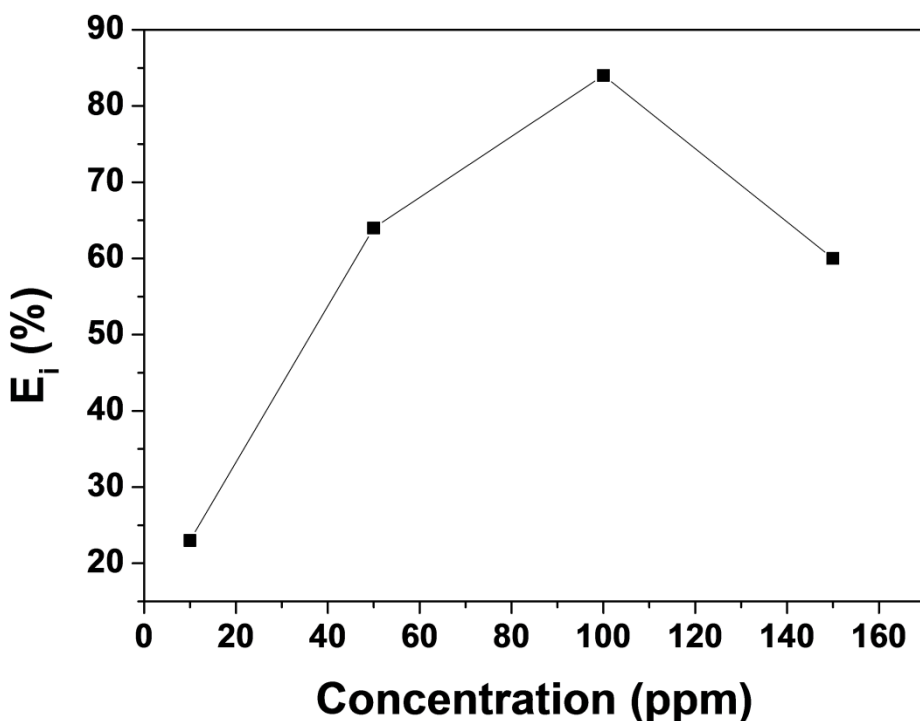


**Figure 4.** The inhibitory efficiency ( $E_i$ ) with different concentrations of the CAC inhibitor.

In the rest of this section, we will study the effect of inhibitor with the critical concentration of 100 ppm.

As we have seen previously, the addition of the inhibitor leads to displace the corrosion potential towards noble values as function of the concentration of the cerium carbonate. Thus, the efficiency of metals corrosion inhibition can be explained by the inhibitor adsorption on metal surface and then the recovery of the metal surface by the molecules of the inhibitor preventing access of corrosive species to metal.

To explain the adsorption mechanism of the CAC inhibitor on the surface of the Brass in 3% NaCl solution, we tried to correlate the experimental results obtained by electrochemical techniques with the plot of the adsorption isotherms.

To describe the adsorption isotherms, several theoretical models have been investigated including Langmuir, Frumkin, Temkin, etc...[44,45] and the most common is that of Langmuir. The Langmuir isotherm assumes that the ability of molecule to bind and adsorb on a given surface is independent of whether or not neighboring sites are occupied. This mean, there will be no interactions

between adjacent molecules on the surface and immobile adsorption. Therefore, adsorption energy is assumed constant.

The free energy of activation ( $\Delta G^\circ_{\text{ads}}$ ) is given by:

$$\Delta G^\circ_{\text{Ads}} = -RT \ln(K) \quad (13)$$

Where R is the universal gas constant, T is the temperature and K is the constant of the adsorption process.

Starting from these assumptions, and for a given temperature, the relationship between the adsorbed quantity of a species and its concentration in the liquid phase which is in contact with the surface is given by the following equations [46]:

$$\frac{\theta}{1-\theta} = KC_{\text{inh}} \quad (14)$$

Or

$$\frac{C_{\text{inh}}}{\theta} = \frac{1}{K} + C_{\text{inh}} \quad (15)$$

Where  $C_{\text{inh}}$  is the concentration and  $\theta$  is the degree of surface coverage.

The degree of surface coverage, ( $\theta$ ), at different concentrations of the CAC which prevents access to the corrosive species and thus blocking the active sites was calculated from the corresponding electrochemical polarization measurements according to [47]:

$$\theta = \left(1 - \frac{I_{\text{corr(inh)}}}{I_{\text{corr}}}\right) \quad (16)$$

Where,  $I_{\text{corr (inh)}}$  and  $I_{\text{corr}}$  is the corrosion current densities without and with addition of the inhibitor, as determined by intersection of the cathode and anode of the straight branches of the Tafel corrosion potential.

The resulting values of recovery rate ( $\theta$ ), reported in Table 1, were used to determine the best isotherm that describes the CAC adsorption method at room temperature.

A linear relationship can be obtained on plotting  $C/\theta$  as a function of C, with a slope of unity, and the value of the intercept is the reciprocal of K. The results of the adsorption of CAC on Brass in 3% NaCl solution are presented in Fig. 5.

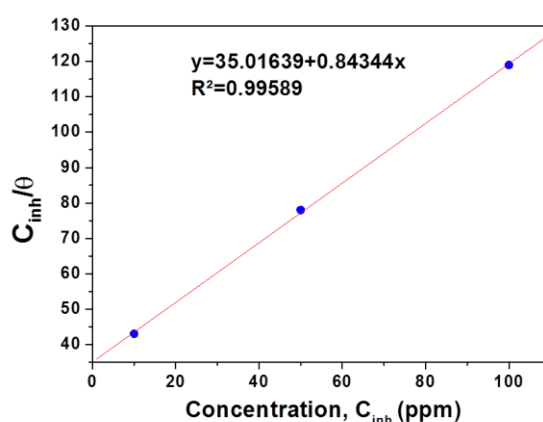


**Figure 5.** Adsorption isotherm for the adsorption of CAC on Brass in 3% NaCl solutions at room temperature.

Fig. 5 shows the correlation between  $C_{inh}/\theta$  and C of the CAC inhibitor. This correlation indicates that the adsorption of the CAC on the Brass surface follows the Langmuir adsorption isotherm. The Adjustment of this correlation by a straight line gives a slope of 0.84, suggesting that each CAC molecule occupies about 84% of the adsorption sites on the Brass surface. The correlation coefficient ( $R_2$ ) is close to 1 ( $> 0.995$ ), confirming the validity of the chosen model.

The corrosion behavior of brass in 3% NaCl solution in the absence and presence of CAC with various concentrations has been additionally studied by electrochemical impedance spectroscopy at room temperature. The electrochemical impedance spectroscopy is now established as a powerful tool for investigating the corrosion mechanisms and inhibitor performance in different environments.

The impedance diagrams in the Nyquist plane of Brass in 3% NaCl without and with different concentrations of CAC inhibitor are shown in Fig. 6. The different impedance parameters are summarized in Table 2.

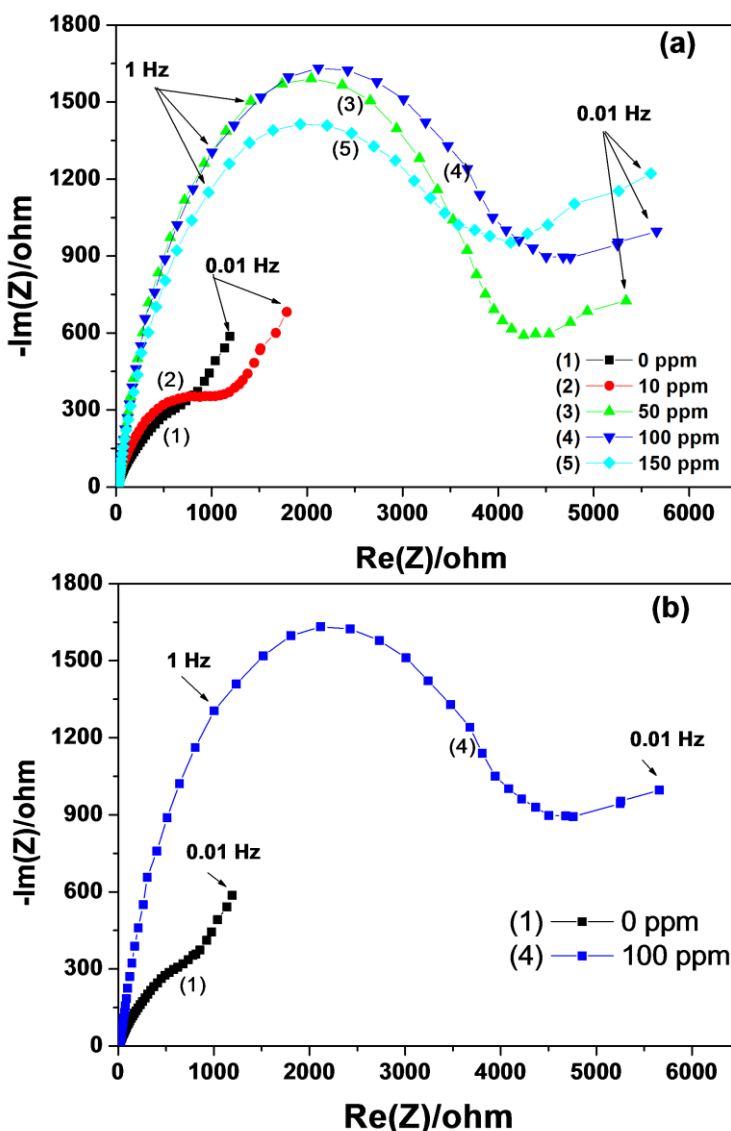


**Figure 6.** Nyquist impedance diagrams of Brass in 3% NaCl solution: (a) in the absence and presence of different concentrations of CAC. (b) In the absence and presence of 100 ppm of CAC.

The Nyquist impedance diagram of Brass in 3% NaCl solution without the CAC inhibitor brings up two distinct fields (high and low frequency). In the field of high frequency, there is a semicircle characterizing a capacitive loop. It has been reported that the semicircles at high frequencies are generally associated with the relaxation of electrical double-layer capacitors, and the diameters of the high-frequency capacitive loops can be considered as the charge-transfer resistance. This capacitive loop is characterized by a charge transfer resistance ( $R_{tc}=1.168\text{K}\Omega$ ) and a double layer capacitor ( $C_{dl}=996\mu\text{F.cm}^{-2}$ ). The linear region at low frequencies could be associated with a diffusional phenomenon in liquid phase [48].

These two phenomena are due to the formation of a porous film consisting of Cu oxides ( $\text{Cu}_2\text{O-CuO}$ ) and zinc oxide ( $\text{ZnO}$ ) [49]. The formation of corrosion products and the Nyquist diagram impedance representation reflect the aggressive attack of chlorides [50]. Moreover, the visible linear branch on the curve (Fig. 6-a) reflects the anodic diffusion process of soluble species such as zinc or copper from the electrode surface into the solution and the cathodic diffusion process of dissolved oxygen from the solution to the electrode surface [51,52].

The values of charge transfer resistance ( $R_{ct}$ ) are calculated from the difference in impedance at high and low frequencies on the real axis [53]. The value of the double layer capacitor ( $C_{dl}$ ) is determined at characteristic of the frequency from the equation:

$$f(-Z_{im}) = \frac{1}{2\pi * C_{dl} R_{tc}} \quad (17)$$

In this study, the modeling of the equivalent circuit and the chemical parameters calculation has been made with the ZView 3.2 software.

Impedance spectra of the Brass in the presence of CAC are different from those without inhibitor, which reflect a modification of the electrochemical process. At high frequency, the diameter of the capacitive loop gradually increases with the CAC concentration to reach a maximum at 100 ppm (Fig. 6-b). At low frequency region, we observed the disappearance of the Warburg diffusion and the beginning of a second loop which corresponds to the adsorption phenomenon of the inhibitor.

**Table 2.** Electrical parameters obtained from the electrochemical impedance spectra of Brass in 3% NaCl solution containing different concentrations of CAC.

Concentration (ppm)	$R_e$ (ohm .cm <sup>2</sup> )	$R_{tc}$ (Kohm.cm <sup>2</sup> )	$C_{dl}$ ( $\mu\text{F.cm}^{-2}$ )	$E_i$ (%)
0	7.30	1.168	996	-
10	7.10	1.292	289	10%
50	8.30	3.930	72	70%
<b>100</b>	<b>7.35</b>	<b>4.480</b>	<b>89</b>	<b>74%</b>
150	7.15	3.725	116	69%

Fig. 7 shows the Bode impedance diagram. In Fig. 7-a, we notice the absence of the linear branch at low frequencies and the presence of two time constants at intermediate and low frequencies for the different CAC concentrations. In addition, we notice that the phase angle reaches maximum values at intermediate frequencies. This maximum increases with the concentrations of CAC until 100

ppm and then it decreases for the highest concentration of inhibitor. These results agree with Nyquist results and demonstrate the adsorption of cerium on the metal surface. In fact, at 150 ppm the surface recovery rate decreases, this is due to the saturation of the site occupied by the CAC molecules.

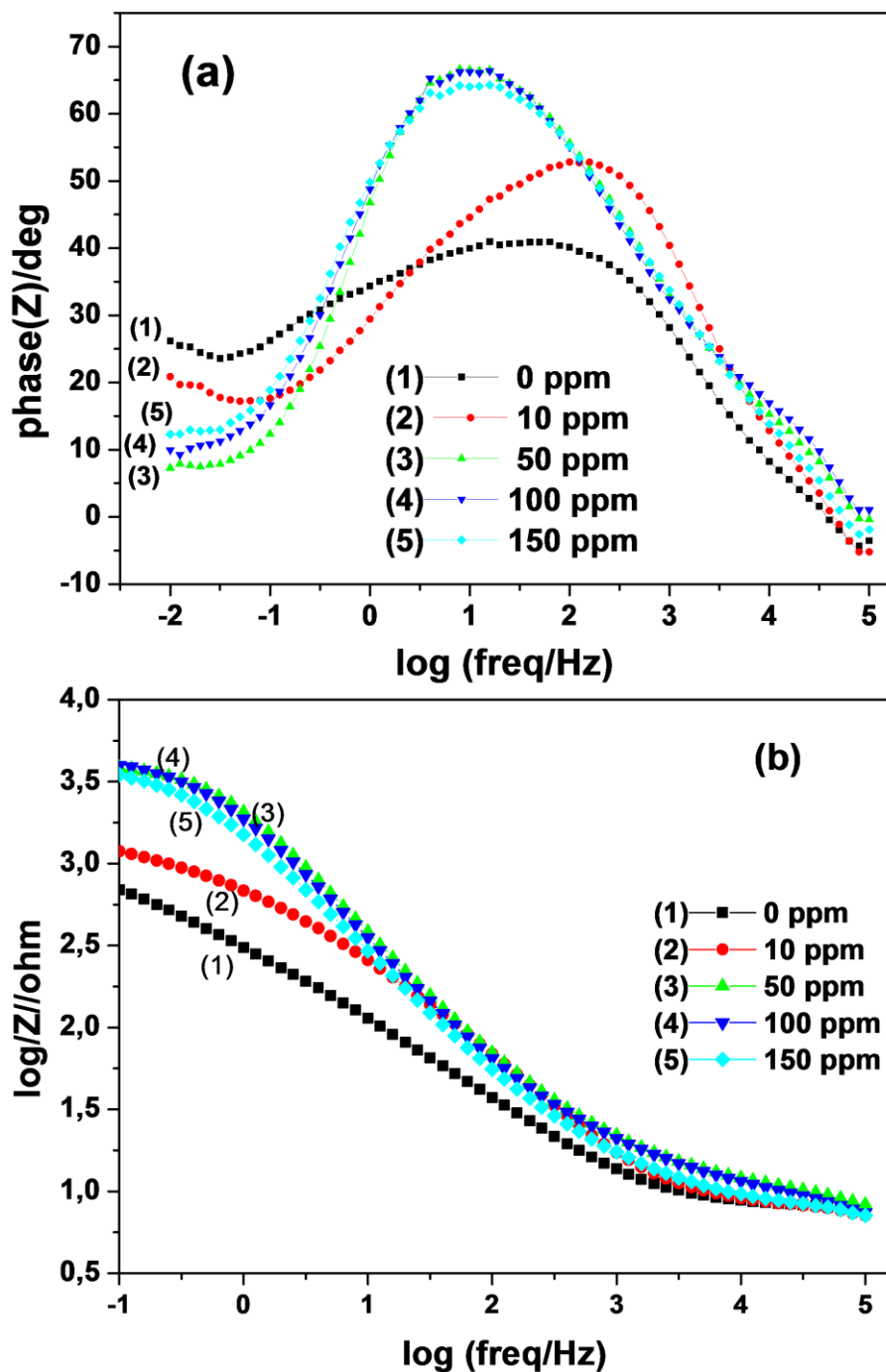


**Figure 7.** Impedance diagrams in the Bode plane of Brass in 3% NaCl solution in the absence and presence of the CAC inhibitor with different concentrations: (a) representation of the phase as a function of frequency and (b) representation of a frequency module function.

The analysis of the Bode diagram (Fig. 7-b) shows that the charge transfer resistance  $R_{ct}$  obtained from the impedance module at low frequency increases gradually with the concentration of CAC. The analysis of the parameters relating to electrochemical impedance measurements (Table 2) of

Brass in 3% NaCl in the absence and presence of CAC shows that the charge transfer resistance  $R_{ct}$  increases with the inhibitor concentration, whereas  $C_{dl}$  decreases as the concentration of CAC increases.

Generally, the concentration of inhibitor increases the recovery rate of the surface and the film thickness. Indeed, the inhibitory effectiveness increases with the inhibitor concentration to achieve 76% at 100 ppm and confirm the results of potentiodynamic study.

The inhibitory efficiency  $P$  was calculated according to the following equation [54]:

$$P = \frac{R_{ct(inh)} - R_{ct}}{R_{ct(inh)}} * 100 \quad (18)$$

Where:

$R_{ct(inh)}$  and  $R_{ct}$  are the values of charge transfer resistance in the presence and absence of the inhibitor, respectively.

The inhibition mechanism of Brass against corrosion in 3% NaCl medium by CAC can be modeled by an equivalent electrical circuit (Fig. 8). This model takes into account the electrical values (Table 2) including the transfer resistance load  $R_{tc}$ , the double layer capacitor ( $C_{dl}$ ), the resistance of Warburg (W) describing the diffusion process Brass without CAC.

The analysis of the diagram allows the measurement at high frequencies of the electrolyte resistance  $R_e$ .

AC impedance results were interpreted using an equivalent circuit in which a constant phase element (CPE) was used in place of a double layer capacitance ( $C_{dl}$ ) in order to give more accurate fit to the experimental results.

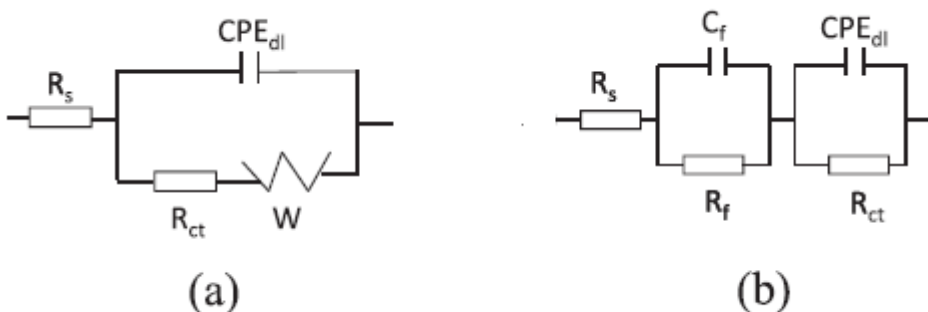


**Figure 8.** Equivalent electrical circuit models representing at high frequency, the Brass / electrolyte interface, (a) in the absence of CAC (b) in the presence of CAC.

### 3.2 Mass loss

#### 3.2.1 Corrosion Rate

The corrosion rate calculated from weight loss after 15 days of immersion in 3% NaCl solution are 46.6  $\mu\text{m}/\text{year}$  in the absence of CAC and 13.1  $\mu\text{m}/\text{year}$  in the presence of CAC. This result confirmed that the presence of CAC decrease the corrosion rate of Brass and lead to protect them from further corrosion by forming a passive layer.

In the previous section, we suggested by electrochemical techniques, the formation of a passive film on the Brass in 3% NaCl medium in the presence of cerium carbonate (CAC). However, the determination of the chemical composition of the film requires the use of other complementary techniques of surface analysis such as SEM and Raman spectroscopy.

### 3.2.2 SEM analysis

Fig. 9 shows the SEM images of the pristine Cu-Zn reference and those of Brass after 15 days of immersion at free corrosion potential in 3% NaCl solution with the absence and presence of the cerium carbonate.

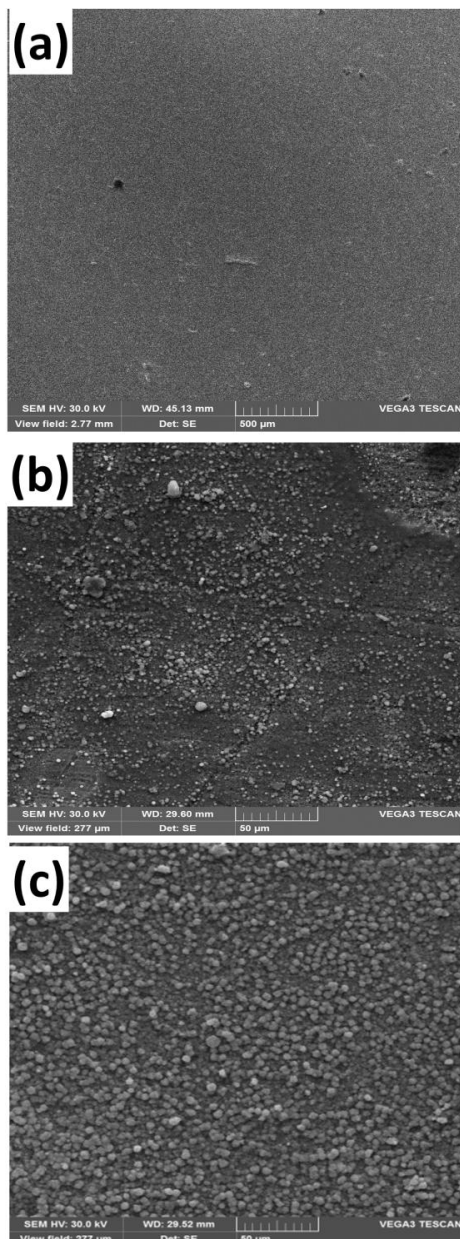


**Figure 9.** SEM images of Brass (a) reference (b) after 15 days of immersion in 3% NaCl solution, (c) after 15 days of immersion in 3% NaCl solution with the CAC inhibitor.

Fig. 9 shows the formation of a corrosion layer on the surface of the Brass, cultivated at  $E_{corr}$  for long periods, under and without the effect of CAC.

In the absence of CAC, the morphology of the oxide layer grown is not homogeneous having a porous structure attributed to the dezincification phenomenon of Brass [55]. The EDX analysis performed on this region revealed the presence of oxygen, copper, zinc, oxygen and chlorides. This is likely due to the formation of the oxide and hydroxide compounds. In the presence of CAC, the inhibiting layer, which covers completely the Brass surface, appears homogeneous and compact.

The compositions of the layer formed in both cases are summarized in Table 3. The results show that the Brass immersed in presence of CAC is enriched in Ce while in the absence of CAC a relatively higher concentration of O and Cl were detected.

By comparing these results with those of electrochemical studies, we can see a clear effect of Brass protection by the formation of a layer containing cerium.

**Table 3.** elemental chemical composition of Brass (in atomic %): immersed for 15 days in 3% NaCl in the absence and presence of the cerium carbonate.

Elements	Brass	After 15 days of immersion in 3% NaCl solution	
		Absence of CAC	Presence of CAC
Cu	76.3%	76.7%	77.1%
Zn	20.7%	15.7%	18 %
Al	2.9%	1.6%	1.5%
Co	<1%	<1%	<1%
O		1.6%	1.2%
C		<1%	<1%
Cl		3%	1.3%
Ce		-	<b>1%</b>

### 3.2.3 Solution analysis

The Brass coupons were immersed in 3% NaCl solution, in the absence and presence of CAC (100 ppm) at room temperature (25 °C) for 15 days.

The solutions were analyzed by ICP-MS to determine the concentration of Cu and Zn leached from the submerged samples. The numerical values of weight loss (NL) measured after 15 days of immersion and the factor corresponding to dezincification (DZ) are presented in Table 4.

The dezincification factor (DZ) was calculated using the following formula [56]:

$$DZ = \frac{\left(\frac{Zn}{Cu}\right)_{sol}}{\left(\frac{Zn}{Cu}\right)_{all}} \quad (19)$$

Where:

(Zn/Cu) sol. : the concentration ratio of Zn / Cu in solution.

(Zn/Cu) all. : the ratio of Zn / Cu in the alloy (% weight).

**Table 4.** Results of the solution analysis by ICP-MS, in the absence and presence of the inhibitor (CAC).

	Solution		Dezincification Factor (DZ)	Inhibition (%)	
	Cu (g/m <sup>2</sup> )	Zn (g/m <sup>2</sup> )		Cu	Zn
Absence of CAC	0.47	5.17	40.0	-	-
Presence of CAC	0.32	0.94	11.3	32%	82%

The results of the solution analysis revealed that both copper and zinc are present in the solution. Nevertheless, we can show that the zinc is preferably released compared to copper, which is in good agreement with elemental chemical composition determined by EDX. Indeed, it is expected that selective corrosion or selective leaching will occur in the case of Brass. Selective corrosion occurs in solid solution alloys when one element or constituent is clearly less noble than the other parts of the material. Generally, any metal with a more negative potential will be preferentially dissolved in the solution, which is the case of Zn compared to Cu.

The weight loss ratio of the Cu/Zn in solution is lower compared to that in the bulk alloy. We could then conclude that the development of the film on the Brass surface and the dissolution of the alloy are controlled by a diffusion process, [57] due to the ionic radius of Zn<sup>2+</sup> (0.07 nm) lower than that of Cu<sup>2+</sup> (0.096 nm) [58].

In conclusion, the inhibitor slowed down the copper and zinc dissolution by controlling the dezincification of Brass in 3% NaCl solution.

The pH remained stable at 7.5 in both experiments indicating that the pH does not play any role on corrosion kinetics.

The calculated values of the inhibition efficiency obtained from the weight loss are shown in Table 4. The inhibitory effectiveness against the dissolution of zinc is higher (82%) compared to the dissolution of copper (32%), indicating that the addition of the CAC inhibitor has an effect on the selective Brass dissolution.

The results of the analysis by ICP-MS solution showed that the CAC effectively controls the dezincification of Brass. The presence of CAC inhibitor (100 ppm) leads to a reduction of the dezincification factor from 40 to 11.3.

### 3.2.4 Raman analysis

Raman spectroscopy is an effective tool to investigate the structure of corroded alloys and steels [59,60]. In this study, Raman measurements were carried out to identify the composition and the nature of different corrosion products observed by electron microscopy.

Fig. 10 shows the Raman spectrum of the CAC inhibitor collected in the wavenumber range 100-2000 cm<sup>-1</sup>. The analysis of the spectrum clearly shows the presence of CeO<sub>2</sub> and CO<sub>3</sub><sup>2-</sup> vibration modes. Spanier et al. [61] reported Raman first-order signals of CeO<sub>2</sub> with an intense peak at 464 cm<sup>-1</sup> which was typically assigned to the T<sub>2g</sub> mode of the Ce-O vibrational unit with Oh symmetry, a broad band between 550 and 600 cm<sup>-1</sup> and two weak second-order peaks at 261, 368 and 1184 cm<sup>-1</sup>. We note also the presence of carbonate bands in the 800-1500 cm<sup>-1</sup> range with the intense v<sub>1</sub> mode at 1360 cm<sup>-1</sup>, and the less intense v<sub>2</sub> and v<sub>3</sub> modes at 845 cm<sup>-1</sup> and 1080 cm<sup>-1</sup> [62].

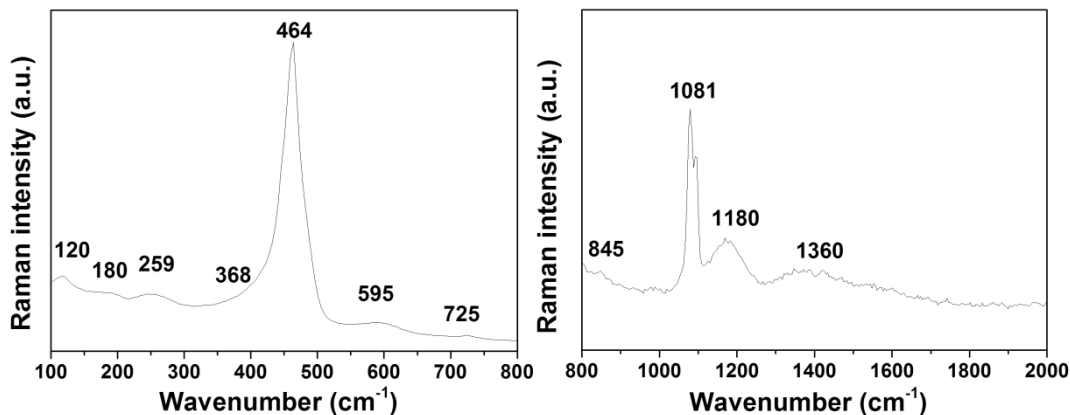


**Figure 10.** Raman spectrum of CAC showing vibrational modes of Ce-O and that of carbonate.

For a more precise determination of phase composition of the layer formed on Brass surface in the absence and presence of CAC inhibitor, Raman investigations were carried out on corroded surfaces (Fig. 11).

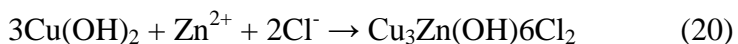
The Raman spectra of the coupon surface in the absence of CAC show the characteristic phonon frequencies of the crystalline Cu<sub>2</sub>O [63]. Indeed, for Cu<sub>2</sub>O, five distinct bands located at 113, 147, 215, 415 and 635 cm<sup>-1</sup> are expected. In addition, the weak peaks observed at 308 and 515 cm<sup>-1</sup> are commonly assigned to the second-order modes of Cu<sub>2</sub>O. The Raman investigations reveal also the presence of the ZnO characterized by the intense vibration mode E<sub>2</sub> at 436 cm<sup>-1</sup>. The low intensity bands were observed at 330, 516, 576, and 650 cm<sup>-1</sup>. The peaks at 330, 516, and 650 cm<sup>-1</sup> are directly associated with the vibration mode caused by multiple-phonon scattering processes [64] and the peak at 576 cm<sup>-1</sup> corresponds to the LO phonon of the A<sub>1</sub> mode.

The four phonon modes of CuO nanocrystals are observed at 276, 327 and 608 cm<sup>-1</sup> and attributed respectively to the A<sub>g</sub> and B<sub>g</sub> modes [65].

In addition, the Raman analysis confirmed the presence of the bands at 120, 145, 365, 509 and 940 cm<sup>-1</sup> typical of kapellasite (Cu<sub>3</sub>Zn(OH)<sub>6</sub>Cl<sub>2</sub>), [66] which is the metastable polymorph of herbertsmithite. In literature, Kapellasite can be synthesized from ZnCl<sub>2</sub> solution and metallic copper metal [67]. The observation by optical microscopy confirmed the green color of Kapellasite.

The presence of Kapellasite clearly shows interactions between chlorine originating from the medium and the Brass metal, as indicated by the presence of Zn<sup>2+</sup> and Cu<sup>2+</sup> in solution (ICP-MS

analysis). The formation of Kapellasite may be due to chemical reactions involving the chloride complexes  $\text{ZnCl}_2$  and  $\text{Cu}(\text{OH})_2$ , according to the reaction:



In the presence of CAC inhibitor, our investigations show similar spectra for  $\text{CuO}$ ,  $\text{Cu}_2\text{O}$  and kapellasite. However, in the presence of CAC, Raman measurements reveal additional vibration modes of cerium ( $264$ ,  $464$  and  $595\text{ cm}^{-1}$ ) mixed with those of kapellasite. It's also important to notice that the Raman vibrational modes attributed to  $\text{ZnO}$  and carbonate ions were not detected suggesting the excellent inhibition efficiency of CAC related to the incorporation of cerium in the corrosion film formed on the alloy surface, which seems to prevent the dissolution of zinc.

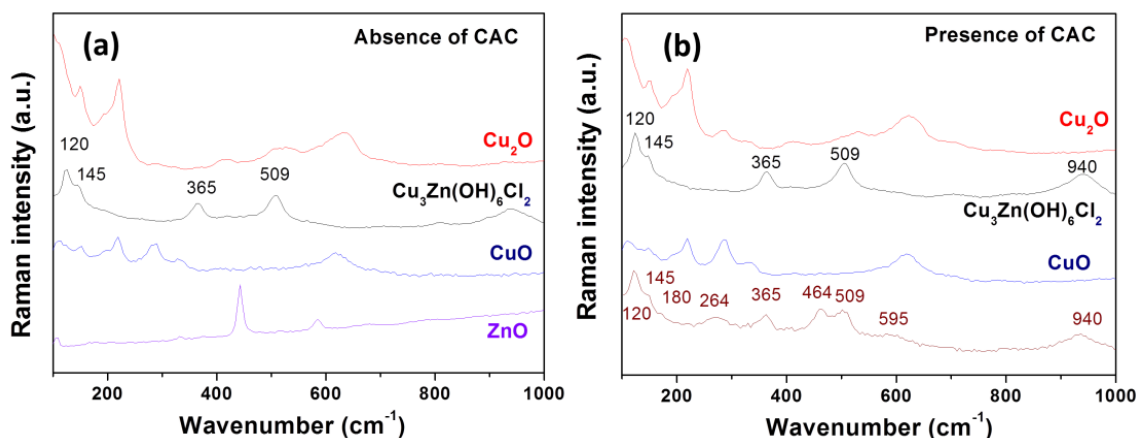


**Figure 11.** Raman spectra of the corrosion products formed on the Brass surface after 15 days in 3%  $\text{NaCl}$  solution (a) in the absence of CAC inhibitor, (b) in the presence of 100 ppm of the CAC inhibitor.

By comparing the Raman results with those of electrochemical studies observations, we can conclude that the CAC present a high protective effect against Brass corrosion by the formation of a dense layer containing cerium. According to our experimental conditions, we can noticed that Ce precipitates as highly insoluble  $\text{Ce}(\text{OH})_4$  or hydrated Ce-oxide ( $\text{CeO}_2 \cdot 2\text{H}_2\text{O}$ ). It is likely that this dense layer inhibited the diffusion of Zn atom from Brass into the solution and thus increased the corrosion resistance. The precipitation of kapellasite in absence (corrosion rate =  $46.6\text{ }\mu\text{m/year}$ ) and presence (corrosion rate =  $13.1\text{ }\mu\text{m/year}$ ) of CAC indicates that this phase does not play a significant protective role against Brass corrosion.

#### 4. CONCLUSION

The present study clearly showed that application by immersion of the ‘green’ corrosion inhibitor cerium carbonate (CAC) presents a high protective effect against the brass corrosion in 3%

NaCl medium. Indeed, the electrochemical measurements showed that the cerium carbonate inhibitory efficiency reached 84% at 100 ppm. The inhibitory effectiveness against the zinc dissolution is higher (82%) compared to the dissolution of copper (32%) and the weight loss measurements showed that the brass corrosion rate decreases by a factor of 3.5 in the presence of CAC after 15 days of experiment. The impedance study revealed that the charge transfer resistance  $R_{tc}$  increases with the concentration of the CAC inhibitor, while the double layer capacitance  $C_{dl}$  decreases as the amount of CAC increases, which is explained by the adsorption phenomenon of the inhibitor on the metal surface. The results of SEM/EDX and Raman investigations confirmed the changes in the brass surface composition after addition of CAC. The presence of cerium hydroxide within the formed film leads to its compactness, thus limiting dezincification. Finally, the use of CAC as a corrosion inhibitor could constitute a promising technique to limit brass corrosion in saline environment.

#### ACKNOWLEDGEMENTS

Special thanks to Abdenour Kabir, research professor (Université du 20 Aout 1955 de Skikda-Algeria) for his help and especially for the SEM measurements.

#### References

1. M. M. Antonijevic and M. B. Petrovic, *Int. J. Electrochem. Sci.*, 3 (2008) 1
2. S. Yadav, A. Sharma, G. Choudhary, Monika, A. Sharma, *Int. J. Innov. Research. Sci. Engin. Tech.*, 3 (2014) 16127
3. M. V. Tomić, M. G. Pavlović, M. Jotanović and R. Fuchs-Godec, *Quality of Life*, 1 (2010) 72
4. A. M. Zaky, *Br. Corros. J.*, 36 (2001) 59
5. M. M. Osman, *Mater. Chem. Phys.*, 71 (2001) 12
6. M. A. Quraishi, I. H. Farooqi and P. A. Saini, *Br. Corros. J.*, 35 (2000) 78
7. H. Imai, Y. Kosaka , A. Kojima, S. Li, K. Kondoh, J. Umeda and H. Atsumi, *Powder Technology*, 198 (2010) 417
8. L. Yohai, M. Vazquez and M. B. Valcarce, *Corros. Sci.*, 53 (2011) 1130
9. O. R. Adetunji, P. O. Aiyyedun, S. I. Kuye, D. A. Lateef, *J. Min. Mater. Charact. Eng.*, 2 (2014) 176
10. R. Nishimura and T. Yoshida, *Corros. Sci.*, 50 (2008) 1205
11. M. Kutz, Mechanical Engineers' Handbook, Materials and Engineering Mechanics, John Wiley & Sons, 2015.
12. Cheng- Kuo Lee, *Int. J. Electrochem. Sci.*, 7 (2012) 8487
13. L. Babouri, K. Belmokre, A. Kabir, A. Abdelouas, Y. El Mendili, *J. Chem. Pharm. Research*, 7 (2015) 1175.
14. N. K. Allama and E. A. Ashour, *Mat. Sci. Eng. B-Solid*, 156 (2009) 84
15. S. Mamas, T. Kyak, M. Kabasakaloglu and A. Koc, *Mater. Chem. Phys.*, 93 (2005) 41
16. A. A. Al-Amiry, A.A. H. Kadhum, A. H. M. Aloabaidy , A. B. Mohamad, P. S. Hoon, *Materials*, 7 (2014) 662
17. M. A. Dar, *Ind. Lubr. Tribol.*, 63 (2011) 227
18. A. Ghazoui, A. Zarrouk, N. Benzaht, R. Salghi, M. Assouag, M. El Hezzat, A. Guenbour, B. Hammouti, *J. Chem. Pharm. Research*, 6 (2014) 704.
19. A. Dermaj, D. Chebabe, M. Doubi, H. Erramli, N. Hajjaji, M. P. Casaletto, G. M. Ingo, C. Ricciucci, T. de Caro, *Corros. Eng. Sci. Tech.*, 50 (2015) 128
20. H. Tian, W. Li, K. Cao, B. Hou, *Corros. Sci.*, 73 (2013) 281.

21. A. I. Muñoz, J. G. Antón, J.L. Guiñón and V. P. Herranz, *Electrochim. Acta*, 50 (2004) 957
22. Q. J. Xu, G. D. Zhou, H. F. Wang and W. B. Cai, *Anti-Corros. Met. Mater.*, 53 (2006) 207
23. X. Wu, N. Chou, D. Luper, L. C. Davis, *Proceeding of the 13th Annual conference on hazardous, waste research*, Snowbird, pp. 374-382, Utah (1998)
24. M. Lebrini, F. Robert, A. Lecante and C. Roos, *Corros. Sci.*, 53 (2011) 687
25. P. C. Okafor, M. E. Ikpi, I. E. Uwah, E. E. Ebenso, U. J. Ekpe and S. A. Umoren, *Corros. Sci.*, 50. (2008) 2310
26. I. B. Obot, Z. M. Gasem, S. A. Umoren, *Int. J. Electrochem. Sci.*, 9 (2014) 510
27. E. A. Matter, S. Kozhukharov, M. Machkova, V. Kozhukharov, *Mater. Corros.*, 64 (2013) 408
28. S. T. Miao, S. Han, L. Hao, *Adv. Mater. Research*, 881-883 (2014) 1165
29. K. Aramaki, *Corros. Sci.*, 43 (2001) 1573
30. R. N. Singh, S. K. Tiwari and W. R. Singh, *J. Alloys Compd.*, 22 (1992) 1175
31. N. D. Nam, M. Mathesh, B. Hinton, M. J. Y. Tan, Maria Forsyth, *J. Electrochem. Soc.*, 161 (2014) C527
32. K. Aramaki, *Corros. Sci.*, 49 (2007) 1963
33. S. Lin and S. K. Fang, *J. Electrochem. Soc.*, 152 (2005) B54
34. M. F. Montemor, A. M. Simoes and M. G. S. Ferriera, *Progr. Org. coat.*, 44 (2002) 111
35. L. Bazzi, R. Salghi, E. Zine, S. El Issami, S. Kertit and B. Hammouti, *Can. J. Chem.*, 80 (2002) 106
36. J. Neeway, A. Abdelouas, B. Grambow, S. Schumacher, C. Martin, M. Kogawa, S. Utsunomiya, S. Gin, and F. Frugier, *J. Non-Crystalline. solids*, 358 (2012) 2894
37. 37. H. G. Jiang, M. Ruhle and E. J. Lavernia, *J. Mater res.*, 14 (1999) 549
38. A. A.E.L. Warraky, *Br. Corros. J.* 32 (1997) 57
39. V. F. Lucey, *Br. Corros. J.*, 2 (1965) 53
40. Z. Xia and Z. Szklarska-Smialowska, *Corros.*, 46 (1990) 85
41. W. J. Van Ooij, *Surf. Technol.* 6 (1977) 1
42. S. W. Dean,W.D. France, S.J. Katchan, in:W.H. Ailor (Ed.), *Handbook of Testing and Evaluation*, John Wiley, p. 174, New York (1984).
43. M. F. Montemor, A.M. Simoes, M.G.S. Ferriera, *Progr. in Organiccoating*, 44 (2002) 111
44. H. Y. Ma, X.L. Cheng, G.Q. Li, S.H. Chen, Z.L. Quan, S. Y. Zhao and L. Niu, *Corros. Sci.*, 42 (2000) 1669.
45. M. R. Arshadi, M. G. Hosseini and M. Ghorbani, *Br. Corros. J.*, 37 (2002) 76
46. H. Fan, S. Li, Z. Zhao, H. Wang, Z. Shi and L. Zhang, *Corros. Sci.*, 53 (2011) 4273
47. A. M. Alsabagh, M.A. Migahed and H.S. Awad, *Corros. Sci.*, 48 (2006) 813
48. K. M. Ismail and W. A. Badawy, *J. Appl. Electrochem.*, 30 (2000) 1303
49. M. M. Osman, *Mater. Chem. Phy.*, 71 (2001) 12
50. D. V. Val, P. A. Trapper, *Reliability Engineering and System Safety*, 93 (2008) 364
51. G. Baril and N. Pebere, *Corros. Sci.*, 43 (2001) 471
52. G. Baril, C. Blanc and N. Pebere, *J. Electrochem. Soc.*, 148 (2001) B489
53. T. Tsuru, S. Haruyama and B. Gijustu, *J. Japan Soc. Corros. Eng.*, 27 (1978) 573
54. K. F. Khaled, *Corros. Sci.*, 2010, 52, 3225.
55. Q. An, Y. Xin, K. Huo, X. Cai and P. K. Chu, *Mater. Chem. Phys.*, 115 (2009) 439
56. G. Trabanali and A. Garassiti, *Adv. Corros. Sci. Technol.*, 13 (1970) 47
57. W. J. V. Ooij, *Surf. Technol.*, 6 (1977) 1
58. K. Ramji, D. R. Cairns and S. Rajeswari, *Appl. Surf. Sci.*, 254 (2008) 4483
59. Y. El Mendili, A. Abdelouas and J.-F. Bardeau, *Phys. Chem. Chem.Phys.*, 15 (2013) 9197
60. Y. El Mendili, A. Abdelouas and J.-F. Bardeau, *RSC. Advances*, 3 (2013) 15148
61. J. E. Spanier, R. Robinson, F. Zhang, S.-W. Chan, and I. P. Herman, *Phys. Rev. B*, 64 (2001) 245407
62. T. Kloprogge, D. Wharton, L. Hickey and R. L. Frost, *Am. Mineral.*, 87 (2002) 623

63. A. Compaan and H. Z. Cummins, *Phys. Rev. B*, 6 (1972) 4753
64. N. Ashkenov, B. N. Mbenkum, C. Bundesmann, V. Riede, M. Lorenz, D. Spemann, E. M. Kaidashev, A. Kasic, M. Schuber, M. Grundmann, G. Wagner, H. Neumann, V. Darakchieva, H. Arwin and B. Monemar, *J. Appl. Phys.*, 93 (2003) 126
65. T. Yu, X. Zhao, Z. X. Shen, Y. H. Wu and W. H. Su, *J. Crystal Growth*, 268 (2004) 590
66. G. G. Rotondo, L. Darchuk, M. Swaenen and R. Van Grieken, *J. Anal. Sci. Method. Instrum.*, 2012, 2, 42
67. R. H. Colman, C. Ritter and A. S. Wills, *Chem. Mater.*, 20 (2008) 6897

© 2015 The Authors. Published by ESG ([www.electrochemsci.org](http://www.electrochemsci.org)). This article is an open access article distributed under the terms and conditions of the Creative Commons Attribution license (<http://creativecommons.org/licenses/by/4.0/>).